AIP | Applied Physics Letters

High-power narrow-vertical-divergence photonic band crystal laser diodes with optimized epitaxial structure

Lei Liu, Hongwei Qu, Yun Liu, Yejin Zhang, Yufei Wang, Aiyi Qi, and Wanhua Zheng

Citation: Applied Physics Letters **105**, 231110 (2014); doi: 10.1063/1.4903883
View online: http://dx.doi.org/10.1063/1.4903883
View Table of Contents: http://scitation.aip.org/content/aip/journal/apl/105/23?ver=pdfcov
Published by the AIP Publishing

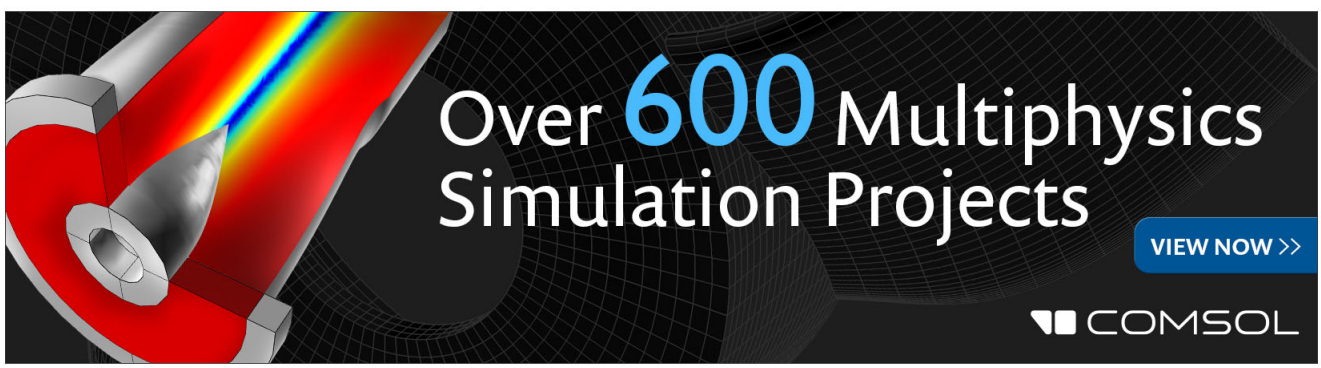

High-power narrow-vertical-divergence photonic band crystal laser diodes with optimized epitaxial structure

Lei Liu,[1,2] Hongwei Qu,[1,2] Yun Liu,[1,2] Yejin Zhang,[1,2] Yufei Wang,[2] Aiyi Qi,[2] and Wanhua Zheng[1,2,a)]

[1]*State Key Laboratory on Integrated Optoelectronics, Institute of Semiconductors, CAS, Beijing 100083, China*
[2]*Laboratory of Solid State Optoelectronics Information Technology, Institute of Semiconductors, CAS, Beijing 100083, China*

(Received 14 August 2014; accepted 21 November 2014; published online 9 December 2014)

900 nm longitudinal photonic band crystal (PBC) laser diodes with optimized epitaxial structure are fabricated. With a same calculated fundamental-mode divergence, stronger mode discrimination is achieved by a quasi-periodic index modulation in the PBC waveguide than a periodic one. Experiments show that the introduction of over 5.5 μm-thick PBC waveguide contributes to only 10% increment of the internal loss for the laser diodes. For broad area PBC lasers, output powers of 5.75 W under continuous wave test and over 10 W under quasi-continuous wave test are reported. The vertical divergence angles are 10.5° at full width at half maximum and 21.3° with 95% power content, in conformity with the simulated angles. Such device shows a prospect for high-power narrow-vertical-divergence laser emission from single diode laser and laser bar. [http://dx.doi.org/10.1063/1.4903883]

Edge-emitting laser diodes are key components in a wide range of applications because of their high wall-plug efficiency (WPE) up to 70%[1,2] and high lifetest time of over thousands of hours.[3] The laser diodes at the wavelengths of (905 ± 10) nm have various applications such as pumping fiber lasers and integrated with silicon detector for an information system due to the sensitivity of silicon detector to this wavelength range. However, they usually have a very large divergence angle (~40°) in the fast axis, which restricts their applications. Several designs have been introduced to reduce the transverse divergence such as the asymmetric waveguide,[4,5] the super large optical cavity (SLOC),[6,7] the graded index double barrier separate confinement heterostructure,[8] the passive far-field reduction layer,[9] the slab-coupled optical waveguide,[10] the plasmonic collimators,[11,12] and the longitudinal photonic band crystal (PBC) waveguide.[13] Among them, only SLOC and longitudinal PBC designs demonstrate continuous wave (CW) power over 1 W and vertical divergence angle less than 10° at full width at half maximum (FWHM), and they have both advantages and disadvantages. For SLOC design, the thick waveguide with a uniform material composition reduces the epitaxial complexity compared to the alternative layer growth of longitudinal PBC design. But its optical losses and series resistance are larger than those of asymmetric waveguide design,[14,15] which is not beneficial for high-power and high efficiency output. For longitudinal PBC design, although the vertical far-field pattern (FFP) is usually characteristic with slow attenuate wings,[16] which increase its divergence angle with 95% power content, the asymmetrical near-field profile reduces the free-carrier absorption in p-doped region and is stable with bias because of the index modulation in the PBC layers. The longitudinal PBC lasers have successfully achieved narrow vertical divergence and pulsed output powers of nearly 20 W at various wavelengths.[17–19] However, their CW output powers of the single PBC device were usually limited to less than 3 W, even with a stripe width of 100 μm.[17,18]

In this paper, we present an optimized design of the longitudinal PBC laser which presents both higher output power and improved vertical divergence compared with our previous results.[20] The performance comparison between laser diodes with and without the PBC structure is also reported, and this will provide a guidance to optimize the PBC laser so as to achieve high-power and high-efficiency laser diodes with narrow vertical divergence.

The epitaxial structure of our longitudinal PBC laser is similar to that of our previous design in Ref. 20, except that the thicknesses of the first low-index layer (LIL) of PBC waveguide, the lower waveguide layer, and the upper cladding layer are increased. The thickening of the upper cladding layer aims at reducing the overlap between the mode profiles and contact layer, and that of the lower waveguide layer aims at enhancing the confinement of the fundamental mode in the active region. The thickening of first LIL behaves like a defect of the PBC which breaks the perfect periodic profile of refractive index. Although the concept of quasi-periodic PBC was proposed by modifying the thickness of several layers closest to the substrate,[21] only the mode leakage to the substrate was controlled, which was not sufficient for the mode selectivity. Generally, confinement factor (CF) is a more widely used quality benchmark, since it describes not only the modal gain provided by active region but also the free carrier absorption by doped region. Figure 1(a) shows the CFs and leakage losses of the first five modes and the far-field angle of the fundamental mode as functions of the first LIL thickness, and Figure 1(b) shows the fundamental mode profile as a function of the first LIL thickness. We can see from Figure 1(a) that as the first LIL

a)Author to whom correspondence should be addressed. Electronic mail: whzheng@red.semi.ac.cn.

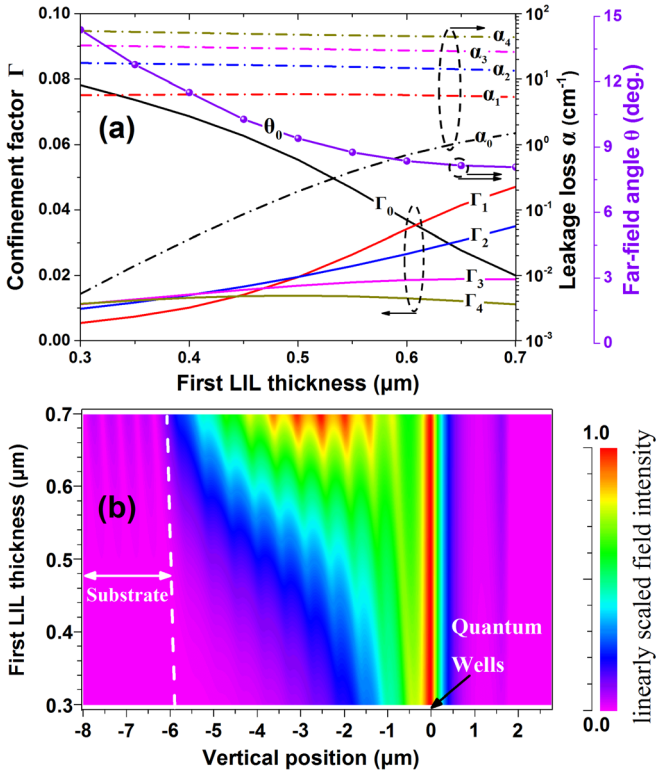

FIG. 1. (a) CFs and leakage losses of the first five modes and the far-field angle of the fundamental mode as functions of the first LIL thickness. (b) Fundamental mode profile as a function of the first LIL thickness.

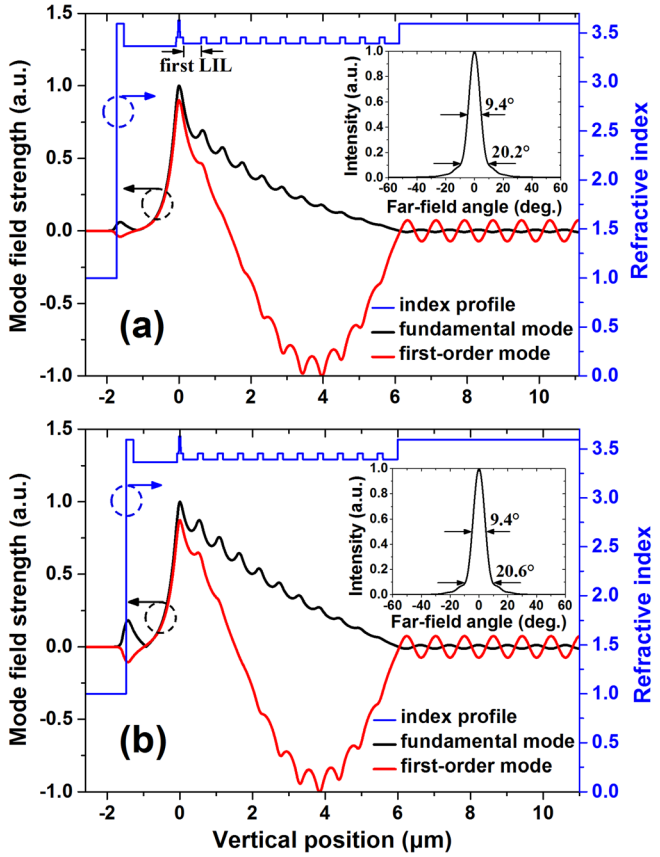

FIG. 2. (a) Refractive index profile and calculated modal field profiles of our optimal PBC epitaxial wafer. (b) Refractive index profile and calculated modal field profiles of our reference PBC wafer in Ref. 20. The insets in (a) and (b) show the calculated vertical FFP of the fundamental mode, and the divergence angles at FWHM and 95% power content are noted.

thickness grows, the fundamental mode and the high-order modes show opposite trends for the confinement factor Γ and leakage loss α. For the fundamental mode, the confinement factor Γ_0 decreases as the first LIL becomes thicker and the trend for the leakage loss α_0 is reverse. This can be demonstrated by the fundamental mode profile which extends towards the substrate as the first LIL thickness increases, as shown in Figure 1(b). The far-field angle of the fundamental mode decreases as the first LIL thickness increases. However, when the first LIL thickness is larger than 0.55 μm, the confinement factor of the 1st order mode Γ_1 are comparable to or even larger than Γ_0, which complicates the mode competition and broadens the total vertical divergence. In addition, the first LIL thickness should be larger than 0.4 μm if the far-field angle of the fundamental mode is designed to be less than 10° (FWHM). Thus, the first LIL thickness should be chosen in the range from 0.45 μm to 0.55 μm. Considering the thickness deviation from design in the epitaxial growth, the optimal value of first LIL thickness should have a design margin and it is chosen to be 0.5 μm. Figures 2(a) and 2(b) show the refractive index and calculated modal field profiles of our optimized PBC wafer and reference PBC wafer in Ref. 20, respectively. From the insets in these figures, we can see that the optimized PBC wafer and reference PBC wafer have comparable far-field angles for the fundamental mode. However, the CF of the fundamental mode is 5.2%, larger than that (3.7%) of our previous design, and the CF ratio of the fundamental mode to high-order modes is 2.6, higher than that (~1.9) of our previous design. This is because the combination of quasi-periodic index modulation with thick lower waveguide layer distinguishes the fundamental mode from the high-order ones more efficiently while maintaining the fundamental mode size. Compared with the periodic PBC design, the fundamental mode is more localized into the active region while maintaining its extended mode size, and the high-order modes are still repelled from the active region, with less gain and higher absorption loss. This stabilizes the low-vertical-divergence operation.

The epitaxial wafer is grown by metal organic chemical vapor deposition on a GaAs substrate, and an optimized doping profile is employed in which the PBC layers close to the active region are low doped. For comparison, a conventional wafer is grown simultaneously, in which the material compositions and thickness of the epitaxial layers are similar to those of our optimal PBC wafer except that the PBC layers are replaced by a typical and uniform AlGaAs waveguide layer. Broad area (BA) waveguides are defined by contact photolithography and the contact layer with a thickness of 200 nm is removed by wet etching. An insulating layer of 250 nm-thick SiO_2 is deposited on the surface and then a contact window is opened on top of the waveguide. Ti/Pt/Au is sputtered on the p-side, followed by deposited a 300 nm-thick gold heat spreader atop the ohmic contact. After the wafer is thinned down to a thickness of 110 μm, Ni/AuGe/Au is evaporated on the n-side. The devices mounted p-side down with indium solder onto a copper heatsink in a TO-3 housing and is tested at room temperature.

Figure 3(a) shows the dependence of the reciprocal differential efficiency on cavity length for the conventional and PBC lasers, respectively. Both devices show high external differential quantum efficiency η_{ex} (over 78% for a cavity length of 600 μm). The PBC device shows internal quantum efficiency η_i of 90% and internal loss α_i of 3.3 cm^{-1}, and the conventional device shows η_i of 92% and α_i of 3.0 cm^{-1}. The difference of η_i may be a measurement or fit artifact, and that of α_i may result from the extra absorption loss of extended mode field by the doped PBC layers. Both differences are very small due to the improved growth of the PBC layers and optimized doping profile. However, the internal loss for PBC laser is large which limits its maximum output power. Some techniques will be conducted in the future to reduce the internal loss, such as increasing the Al content of the upper cladding layer to reduce the overlap of modes with p-doped region. To further compare the characteristics of the conventional and PBC devices, lasers based on both wafers are fabricated, with stripe width of 100 μm, cavity length of 1 mm, and facet coating reflectivities of 95%/6%. Their light-current-voltage (L-I-V) curves under the quasi-CW (QCW) test are presented in Figure 3(b). The slope efficiency of the PBC laser is only slightly lower (~0.08 W/A) than that of the conventional laser mainly because of the extra absorption loss in the PBC waveguide mentioned above. However, the PBC laser shows an obviously larger threshold current (365 mA) than that (278 mA) of the conventional laser. The threshold current of quantum well lasers can be described as

$$I_{th} = W \times L \times J_{tr} \exp\left(\frac{\alpha_i + \frac{1}{2L}\ln(R_f R_r)^{-1}}{\Gamma g_0}\right), \qquad (1)$$

where W and L are the stripe width and cavity length of the laser, respectively, J_{tr} is the transparency current density, Γ is the CF, g_0 is the reference gain, R_f is the front facet reflectivity, and R_r is the rear facet reflectivity. From Eq. (1), the threshold current grows exponentially with the reciprocal CF. Since the CF (~14.5%) of fundamental mode of conventional laser is nearly threefold of that of PBC laser, the increased threshold of PBC laser should be mainly attributed to its reduced CF. Conventional laser shows a series resistances of 440 mΩ, which limits its maximum WPE to below 45%, and PBC lasers show larger series resistances of nearly 500 mΩ limiting it maximum WPE to below 40%. We can also see that the introduction of PBC layers contributes to a resistance increment of only 60 mΩ which is too small to limit the PBC device performances such as the maximum WPE. If we assume that the series intrinsic resistance of n-doped bulk AlGaAs can be ignored, then the average junction resistance per PBC step interface is estimated to be 3 mΩ, comparable to the state of art in distributed Bragg reflector of vertical cavity surface emitting lasers. According to our preliminary analysis, it is the poor metal contact and package that mainly result in so large series resistances (>400 mΩ) of our conventional and PBC lasers. To be competitive with the best other high-power low-divergence edge-emitting lasers with higher WPE (>50%), reducing the series resistance of PBC lasers to lower than 100 mΩ is primary, by methods such as improving the metal contact to reduce the contact resistance or further optimizing the doping profile.

To achieve a higher output power, PBC laser with a stripe width of 200 μm and a cavity length of 1.3 mm is fabricated and the rear and front facets are coated with reflectivities of 95% and 2%, respectively. Figure 4 shows the L-I-V curves under CW and QCW ($\tau = 40\ \mu s$ and f = 40 Hz) operations. The device can deliver output power of 5.75 W in CW mode limited by thermal roll-over, and 10.3 W in QCW mode limited by catastrophic optical mirror damage accelerated by Joule heat.

Since very poor package and measurement conditions are used, we suppose that a much higher CW output power can be achieved by using AuSn solder and improved mounting,[22] and higher pulse power by employing driving current source with short pulse width (<1 μs) and passivated facets.

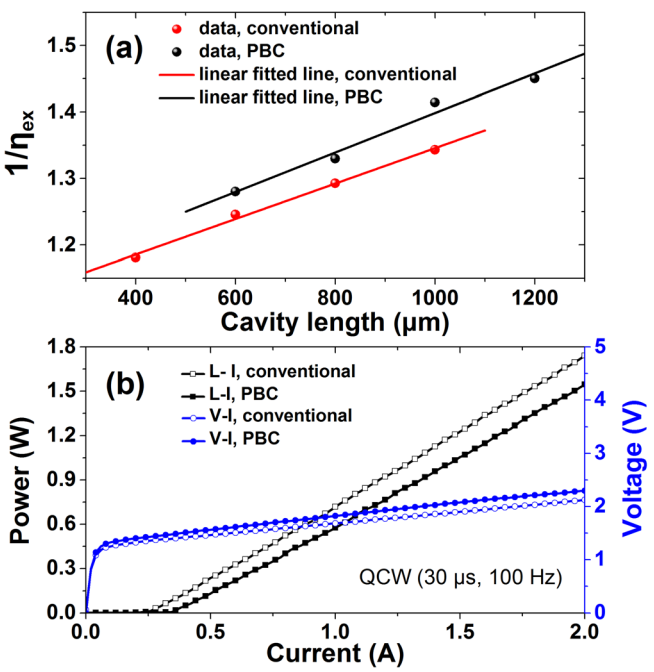

FIG. 3. (a) Dependence of the reciprocal differential efficiency on cavity length for the conventional and PBC lasers, respectively. (b) L-I-V curves of conventional and PBC lasers with a cavity length of 1 mm in QCW mode.

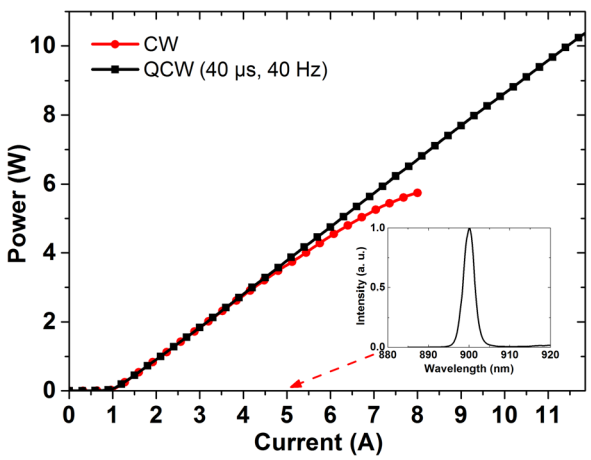

FIG. 4. L-I-V curves under the CW and QCW operations for our PBC lasers with a cavity length of 1.3 mm. The inset shows the measured spectrum at the current of 5 A in CW mode.

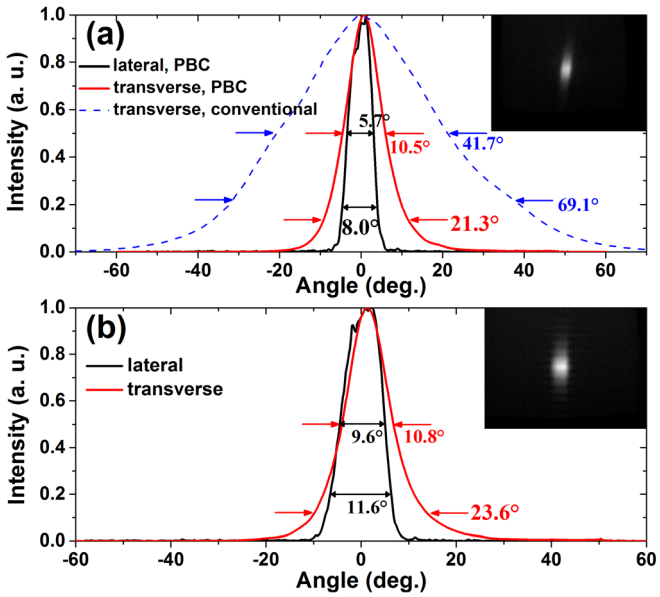

FIG. 5. Transverse and lateral FFPs of our PBC laser in CW (a) and QCW (b) operations, respectively. The insets of (a) and (b) show the 2-D infrared far-field image of the PBC laser, and the blue dashed line in (a) shows the vertical FFP of the conventional laser with a CW output power of 1 W. Divergence angles at FWHM and 95% power content are noted for every profile.

Both operations show a nearly same threshold current of about 1 A, and the slope efficiency under QCW test is 1.02 W/A. The efficiency in CW mode becomes obviously lower than the one in QCW mode when the current exceeds 5 A because of the strong self-heating effect. The optical spectrum is measured at the current of 5 A, with an intensity peak at 900 nm.

Figures 5(a) and 5(b) present the FFPs of the 200 μm-wide PBC device at the CW current of 2 A and QCW current of 8 A, respectively. In CW mode, the transverse FFP with the output power of 1 W shows a divergence of 10.5° at FWHM and 21.3° at 95% power content which are close to those in our simulation. Compared to the transverse divergence of the conventional laser, the divergence of PBC laser has a reduction of 31.2° at FWHM and 48.8° with 95% power content. Moreover, the 95% power transverse angle of our optimal PBC device is greatly reduced compared to that (~50°) of our previous PBC device[20] at the same output level, although their FWHM angles are similar. This is contributed to the strengthened mode discrimination mentioned above, which provides more gain for the fundamental mode and more loss for high-order ones. The lateral FFP presents a single-lobe profile with divergence of 5.7° at FWHM and 8.0° at 95% power content. In QCW operation, the transverse divergence angles are 10.8° at FWHM and 23.6° at 95% power content, which are only slightly larger than those in CW mode although the driving current reaches 8 A. The lateral FFP shows divergence of 9.6° at FWHM and 11.6° at 95% power content, larger than those in CW mode because of the increased current to 8 A.

In conclusion, we have fabricated longitudinal PBC laser diodes with optimized design of PBC layers and doping profile. The PBC laser can achieves similar slope efficiency as those of the conventional laser, with only slightly differences in internal quantum efficiency and internal loss. Record high CW output power of 5.75 W is achieved by our PBC laser, and the experimental vertical far-field divergence agrees with that of the simulated one. Much higher output power can be inferred in the future study if the package and driving conditions are improved.

This work was supported by the Chinese National Key Basic Research Special Fund/CNKBRSF (Grant Nos. 2012CB933501 and 2011CB922002), the National Natural Science Foundation of China (Grant Nos. 61025025, 61137003, and 61021003), and the National High Technology Research and Development Program of China (Grants No. 2012AA012202).

[1]P. Crump, W. Dong, M. Grimshaw, J. Wang, S. Patterson, D. Wise, M. DeFranza, S. Elim, S. Zhang, M. Bougher, J. Patterson, S. Das, J. Bell, J. Farmer, M. DeVito, and R. Martinsen, Proc. SPIE **6456**, 64560M (2007).
[2]M. Kanskar, T. Earles, T. J. Goodnough, E. Stiers, D. Botez, and L. J. Mawst, Electron. Lett. **41**, 245 (2005).
[3]J. Wang, L. Bao, M. DeVito, D. Xu, D. Wise, M. Grimshaw, W. Dong, S. Zhang, C. Bai, P. Leisher, D. Li, H. Zhou, S. Patterson, R. Martinsen, and J. Haden, Proc. SPIE **7583**, 758305 (2010).
[4]A. P. Bogatov, T. I. Gushchik, A. E. Drakin, A. P. Nekrasov, and V. V. Popovichev, Quantum Electron. **38**, 935 (2008).
[5]J. X. Zhang, L. Liu, W. Chen, A. J. Liu, W. J. Zhou, and W. H. Zheng, Chin. Opt. Lett. **10**, 061401 (2012).
[6]A. Pietrzak, P. Crump, H. Wenzel, G. Erbert, F. Bugge, and G. Tränkle, IEEE J. Sel. Top. Quantum Electron. **17**, 1715 (2011).
[7]A. Pietrzak, H. Wenzel, P. Crump, F. Bugge, J. Fricke, M. Spreemann, G. Erbert, and G. Tränkle, IEEE J. Quantum Electron. **48**, 568 (2012).
[8]C. T. Hung and T. C. Lu, IEEE J. Quantum Electron. **49**, 127 (2013).
[9]L. P. Hou, M. Haji, J. Akbar, A. C. Bryce, and J. H. Marsh, IEEE Photon. Technol. Lett. **24**, 1057 (2012).
[10]R. K. Huang, J. P. Donnelly, L. J. Missaggia, C. T. Harris, J. Plant, D. E. Mull, and W. D. Goodhue, IEEE Photon. Technol. Lett. **15**, 900 (2003).
[11]N. F. Yu, J. Fan, Q. J. Wang, C. Pflügl, L. Diehl, T. Edamura, M. Yamanishi, H. Kan, and F. Capasso, Nat. Photonics **2**, 564 (2008).
[12]R. Blanchard, T. S. Mansuripur, B. Gökden, N. F. Yu, M. Kats, P. Genevet, K. Fujita, T. Edamura, M. Yamanishi, and F. Capasso, Appl. Phys. Lett. **102**, 191114 (2013).
[13]N. N. Ledentsov and V. A. Shchukin, Opt. Eng. **41**, 3193 (2002).
[14]K. H. Hasler, H. Wenzel, P. Crump, S. Knigge, A. Maasdorf, R. Platz, R. Staske, and G. Erbert, Semicond. Sci. Technol. **29**, 045010 (2014).
[15]P. Crump, G. Erbert, H. Wenzel, C. Frevert, C. M. Schultz, K.-H. Hasler, R. Staske, B. Sumpf, A. Maaßdorf, F. Bugge, S. Knigge, and G. Tränkle, IEEE J. Sel. Top. Quantum Electron. **19**, 1501211 (2013).
[16]M. V. Maximov, Y. M. Shernyakov, I. I. Novikov, S. M. Kuznetsov, L. Ya. Karachinsky, N. Yu. Gordeev, V. P. Kalosha, V. A. Shchukin, and N. N. Ledentsov, IEEE J. Quantum Electron. **41**, 1341 (2005).
[17]K. Posilovic, T. Kettler, V. A. Shchukin, N. N. Ledentsov, U. W. Pohl, D. Bimberg, J. Fricke, A. Ginolas, G. Erbert, G. Tränkle, J. Jönsson, and M. Weyers, Appl. Phys. Lett. **93**, 221102 (2008).
[18]I. I. Novikov, N. Yu. Gordeev, Yu. M. Shernyakov, Yu. Yu. Kiselev, M. V. Maximov, P. S. Kop'ev, A. Sharon, R. Duboc, D. B. Arbiv, U. Ben-Ami, V. A. Shchukin, and N. N. Ledentsov, Appl. Phys. Lett. **92**, 103515 (2008).
[19]K. Posilovic, V. P. Kalosha, M. Winterfeldt, J.-H. Schulze, D. Quandt, T. D. Germann, A. Strittmatter, D. Bimberg, J. Pohl, and M. Weyers, Electron. Lett. **48**, 1419 (2012).
[20]L. Liu, H. W. Qu, Y. Liu, Y. F. Wang, A. Y. Qi, X. J. Guo, P. C. Zhao, Y. J. Zhang, and W. H. Zheng, IEEE J. Sel. Top. Quantum Electron. **21**, 1900107 (2015).
[21]V. P. Kalosha, K. Posilovic, T. Kettler, V. A. Shchukin, N. N. Ledentsov, and D. Bimberg, Semicond. Sci. Technol. **26**, 075014 (2011).
[22]D. Bimberg, K. Posilovic, V. Kalosha, T. Kettler, D. Seidlitz, V. A. Shchukin, N. N. Ledentsov, N. Y. Gordeev, L. Y. Karachinsky, I. I. Novikov, M. V. Maximov, Y. M. Shernyakov, A. V. Chunareva, F. Bugge, and M. Weyers, Proc. SPIE **7616**, 76161I (2010).